Silicon-based all-optical multi microring network-on-chip

Paolo Pintus,[1,*] Pietro Contu,[1,2] Pier Giorgio Raponi,[1] Isabella Cerutti,[1] and Nicola Andriolli[1]

[1]Scuola Superiore Sant'Anna, 56124 Pisa, Italy

[2]Electrical and Computer Engineering Department, Boston University, Boston, Massachusetts 02215, USA

*Corresponding author: paolo.pintus@sssup.it

An optical multi microring network-on-chip (MMR NoC) is proposed and evaluated through numerical simulations. The network architecture consists of a central resonating microring with local microrings connected to the input/output ports. A mathematical model based on the transfer matrix method is used to assess the MMR NoC performance and to analyze the fabrication tolerances. Results show that the proposed architecture exhibits a limited coherent crosstalk with a bandwidth suitable for 10 Gb/s signals, and it is robust to coupling ratio variations and ring radii fabrication inaccuracies. © 2014 Optical Society of America

OCIS codes: (060.1155) All-optical networks; (130.0130) Integrated optics; (130.4815) Optical switching devices.
http://dx.doi.org/10.1364/OL.39.000797

The current trend in computing platforms is to integrate a large number of cores onto a single die, so that the computational performance can be improved by means of parallelization. The degree of integration is posing new challenges in designing the on-chip interconnection networks, or network-on-chip (NoC), required for core-to-core and core-to-cache communications. The NoC not only must provide high performance in terms of latency and bandwidth (BW), but also must be energy efficient and integrated on the same platform. The current issue with the conventional electronic NoC is that as the number of cores increases the size of the electrical connections, the power dissipation, and the BW are becoming a bottleneck for the performance of the computing systems [1,2]. Photonic solutions can alleviate this limitation, providing increased BW at low power consumption and no electromagnetic interference [1–4]. Thanks to the unique properties of photonic communication (e.g., large BW) and to the advances in photonic integration, photonic NoCs are expected to improve the levels of performance-per-watt achieved by electronic NoCs, making them a suitable candidate for future computing platforms. The potential of photonic NoCs is currently under investigation by various research groups [1,2] leading to the realization of initial prototypes [5].

This Letter presents a novel architecture for photonic NoC, based on microring resonators. Microrings can be used as filters, can offer high modulation speeds at low power consumption, and can be integrated using the silicon-on-isolator (SOI) technology platform. Parallel transmissions on multiple wavelengths are possible by exploiting wavelength division multiplexing. The simultaneous transmission of different signals on the same wavelength is possible provided that their propagating paths are disjoint. The novelty of the proposed integrated optical NoC is the use of resonant microrings for both filtering the ingress/egress signal for add/drop functionalities (i.e., at local microrings), as well as for the communication between the different ingresses and egresses (i.e., in a central microring), leading to a multi microring (MMR) NoC design [6]. Such a design guarantees all-to-all communication while avoiding any waveguide crossings, which are a major source of crosstalk in optical integrated circuits. Although the crosstalk of a single crossing can be as small as −20 dB [5], in NoC where paths have multiple waveguide intersections the signal quality might be seriously impaired. Moreover, the use of local microrings allows for a better filtering of the signal at the receivers, free of interference noise.

A mathematical model is presented for assessing and optimizing the MMR NoC performance. The aim is to validate the feasibility of the proposed MMR NoC when accounting for crosstalk problems and the robustness of the design to fabrication inaccuracies. The considered MMR NoC consists of four transmitters, T_i, and four receivers, R_i, with $i = 1, 2, 3, 4$, each one connected through a waveguide to a local microring of radius r, as shown in Fig. 1. The local microrings are adjacent to a central microring of radius ρ. By setting the radius ρ as a multiple of r (i.e., $\rho = nr$, n integer), the local microrings act as filters and allow the signal to be simultaneously added and dropped. Similarly, the central microring carries the signals on the same resonant frequencies of the other microrings. As an example, assume that a modulated signal is sent from T_1 to R_2, while the other transmitters and receivers are turned off (i.e., $T_1 = $ ON, $T_2 = T_3 = T_4 = $ OFF). The local microrings at T_1 and R_2 and the
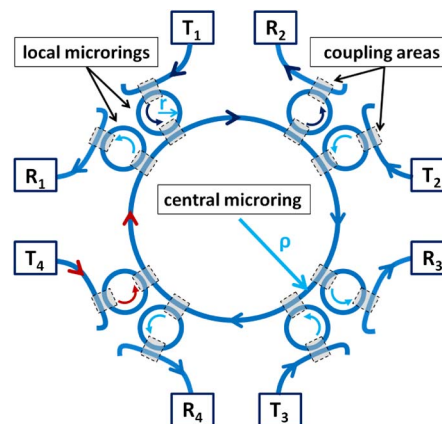
Fig. 1. MMR NoC architecture.

© 2014 Optical Society of America

central microring are tuned on at the same resonance wavelength. The modulated signal generated by T_1 is coupled to the counterclockwise local microrings and then to the central microring. The latter is clockwise resonating and allows the propagation of the signal, which is then dropped at receiver R_2 by the counterclockwise local microring. However, an undesired part of the signal continues its propagation along the central microring reaching the other receivers and leading to crosstalk effects. Therefore, the proposed MMR architecture needs to be optimized with the aim of minimizing the amount of undesired signal or crosstalk, as explained next.

The performance of the MMR NoC is modeled by using the transfer matrix method [7–9], which is more efficient than the finite-difference time-domain method in terms of memory utilization and computational time. To compute the transfer matrix relating the input signals at T_j with the output signals at R_i, the NoC has been divided into four slices or sectors. One of the slices of the MMR NoC is shown in Fig. 2. In the figure, the waveguide connected to the transmitter T_1 (receiver R_1) has an unused or dummy termination DR_1 (DT_1). The behavior of the local microrings in Fig. 2 is described by the scattering matrices $\underline{p}$ and $\underline{q}$ [8], defined as follows:

$$\begin{pmatrix} DR_1 \\ D_1 \end{pmatrix} = \begin{pmatrix} p_{11} & p_{12} \\ p_{21} & p_{22} \end{pmatrix} \begin{pmatrix} T_1 \\ C_1 \end{pmatrix}, \tag{1a}$$

$$\begin{pmatrix} R_1 \\ B_1 \end{pmatrix} = \begin{pmatrix} q_{11} & q_{12} \\ q_{21} & q_{22} \end{pmatrix} \begin{pmatrix} DT_1 \\ A_1 \end{pmatrix}, \tag{1b}$$

where A_1 and C_1 are the signals along the central ring at the positions indicated in the figure and are coupled to local rings of slice 1, whereas B_1 and D_1 are the signals that are coupled back to the central ring. Additionally, the signals in the central ring are linked by the following phase-shift relations: $C_1 = \tau_i B_1$ and $A_2 = \tau_e D_1$, where A_2 is the signal propagating to the next slice. The constant τ_i and τ_e are related to the central angles θ_i and θ_e, respectively, defined as in Fig. 2. By introducing the round-trip transmission factor for the central microring as $\tau = \exp[-(\alpha + j\beta)2\pi\rho]$, where α and β are the attenuation and phase constants, it is possible to derive $\tau_i = \tau^{\theta_i/2\pi}$ and $\tau_e = \tau^{\theta_e/2\pi}$. Moreover, assuming identical slices, $\theta_i + \theta_e = 90°$. It can be shown that

$$\begin{pmatrix} R_1 \\ A_2 \end{pmatrix} = \begin{pmatrix} 0 & q_{12} \\ \tau_e p_{21} & \tau_e p_{22}\tau_i q_{22} \end{pmatrix} \begin{pmatrix} T_1 \\ A_1 \end{pmatrix}. \tag{2}$$
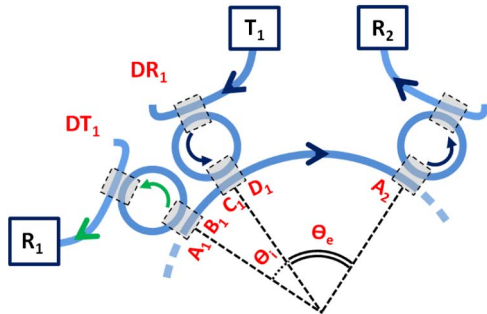
Fig. 2.   Slice 1 of MMR NoC.

Equation (2) relates the input and output (T_1 and R_1) of slice 1 with the signals that propagate in the central microring (A_1 and A_2). Note that the signal outgoing from the slice under investigation is the incoming signal for the next slice. By considering similar relations for all slices, the transfer matrix of the MMR NoC can be computed. For this purpose, let us introduce the following coefficients:

$$s_{12}^{(i)} = q_{12}^{(i)}, \qquad s_{21}^{(i)} = \tau_e^{(i)} p_{21}^{(i)}, \qquad s_{22}^{(i)} = \tau_e^{(i)} p_{22}^{(i)} \tau_i^{(i)} q_{22}^{(i)}, \tag{3}$$

where the superscript (i) with $i = 1, 2, 3, 4$ indicates the corresponding slice numbered in the clockwise direction. As a result, the NoC transfer matrix $\underline{\underline{S}}$ can be computed as

$$\begin{pmatrix} R_1 \\ R_2 \\ R_3 \\ R_4 \end{pmatrix} = \begin{pmatrix} S_{11} & S_{12} & S_{13} & S_{14} \\ S_{21} & S_{22} & S_{23} & S_{24} \\ S_{31} & S_{32} & S_{33} & S_{34} \\ S_{41} & S_{42} & S_{43} & S_{44} \end{pmatrix} \begin{pmatrix} T_1 \\ T_2 \\ T_3 \\ T_4 \end{pmatrix}. \tag{4}$$

The entries of matrix $\underline{\underline{S}}$ are

$$S_{i,i} = s_{12}^{(i)} s_{22}^{(i+3)} s_{22}^{(i+2)} s_{22}^{(i+1)} s_{21}^{(i)}/w, \tag{5a}$$

$$S_{i,i+1} = s_{12}^{(i)} s_{22}^{(i+3)} s_{22}^{(i+2)} s_{21}^{(i+1)}/w, \tag{5b}$$

$$S_{i,i+2} = s_{12}^{(i)} s_{22}^{(i+3)} s_{21}^{(i+2)}/w, \tag{5c}$$

$$S_{i,i+3} = s_{12}^{(i)} s_{21}^{(i+3)}/w, \tag{5d}$$

where the index i is modulo 4 and

$$w = 1 - s_{22}^{(4)} s_{22}^{(3)} s_{22}^{(2)} s_{22}^{(1)}. \tag{6}$$

The transmission coefficients in Eq. (5) depend on the waveguide attenuation (α), the phase constant (β), the ring radii (r and ρ), and the ring–waveguide power coupling ratio (K) defined as the fraction of power coupled to the ring per round trip [8,9]. By generalizing the transmission coefficients S_{ij}, the model can be extended to a MMR NoC with more transmitters/receivers. In designing this NoC, it is important to ensure that K is larger than the surface-roughness-induced reflectivity, so that the backscattering can be considered negligible [10,11].

The worst case scenario from the coherent crosstalk perspective is when all the microrings are resonating at the same wavelength and the communication occurs between adjacent transmitters and receivers. When all the rings are identical, only four of sixteen transmission coefficients S_{ij} need to be defined because of the symmetry. As a result, $\underline{\underline{S}}$ becomes the circulant matrix [12]

$$\begin{pmatrix} R_1 \\ R_2 \\ R_3 \\ R_4 \end{pmatrix} = \begin{pmatrix} S_{11} & S_{12} & S_{13} & S_{14} \\ S_{14} & S_{11} & S_{12} & S_{13} \\ S_{13} & S_{14} & S_{11} & S_{12} \\ S_{12} & S_{13} & S_{14} & S_{11} \end{pmatrix} \begin{pmatrix} T_1 \\ T_2 \\ T_3 \\ T_4 \end{pmatrix}, \tag{7}$$

whose entries are as follows:

$$S_{11} = \frac{s_{12}(s_{22})^3 s_{21}}{1-(s_{22})^4}, \qquad S_{12} = \frac{s_{12}(s_{22})^2 s_{21}}{1-(s_{22})^4},$$

$$S_{13} = \frac{s_{12}(s_{22})^1 s_{21}}{1-(s_{22})^4}, \qquad S_{14} = \frac{s_{12}s_{21}}{1-(s_{22})^4}, \tag{8}$$

where the index (i) is no longer required.

Receiver R_2 receives the signal from T_1 plus three crosstalk contributions from the transmitters T_1, T_2, and T_3, as follows:

$$R_2 = \underbrace{S_{14}T_1}_{\text{signal}} + \underbrace{S_{11}T_2 + S_{12}T_3 + S_{13}T_4}_{\text{crosstalk}}. \tag{9}$$

The crosstalk contribution XT_{1j} $(j = 2, 3, 4)$ at R_2 is defined as the absolute value of the ratio between the interfering signal transmitted by T_j [i.e., the elements $S(2,j)$ in the matrix $\underline{S}$] and the signal transmitted by T_1 [i.e., $S(2,1) = S_{14}$] and is given by

$$XT_{12} = \frac{|R_2|^{T_2=1}_{T_1=T_2=T_3=0}}{|R_2|^{T_1=1}_{T_2=T_3=T_4=0}} = \frac{|S(2,2)|}{|S(2,1)|} = \left| \frac{S_{11}}{S_{14}} \right|, \tag{10}$$

$$XT_{13} = \frac{|R_2|^{T_3=1}_{T_1=T_2=T_4=0}}{|R_2|^{T_1=1}_{T_2=T_3=T_4=0}} = \frac{|S(2,3)|}{|S(2,1)|} = \left| \frac{S_{12}}{S_{14}} \right|, \tag{11}$$

$$XT_{14} = \frac{|R_2|^{T_4=1}_{T_1=T_2=T_3=0}}{|R_2|^{T_1=1}_{T_2=T_3=T_4=0}} = \frac{|S(2,4)|}{|S(2,1)|} = \left| \frac{S_{13}}{S_{14}} \right|. \tag{12}$$

To assess the performance, a SOI platform with 450 nm × 220 nm transverse electric (TE) single-mode silicon waveguides is considered with microring radii $r = 10$ μm and $\rho = 40$ μm. The phase constants are computed using a full vectorial finite element solver [13], while the attenuation is $\alpha = 11.5$ dB/cm [11,14]. Moreover, the coupling areas (gray squares in Fig. 1) are assumed to be identical and K is proportional to $1/\lambda^2$ [15]. Figure 3 shows the spectral response of S_{11}, S_{12}, S_{13}, and S_{14} for $K = 10\%$. The solid (dashed) vertical lines indicate the resonant wavelengths of the local (central) microrings. In addition, the free spectral range of the local (central) microrings are reported as fsr (FSR). For $\lambda = 1536.04$ nm, the amplitude of S_{14} is close to 0 dB, allowing the transmission from T_1 to R_2, whereas S_{11}, S_{12}, S_{13} are approximatively 40 dB lower at the same resonant wavelength. The crosstalk contributions XT_{12}, XT_{13}, and XT_{14} with respect to K within the 3 and 1 dB BW of S_{14} are shown in Figs. 4(a) and 4(b), respectively. The major contribution to the overall crosstalk at receiver R_2 is caused by transmitter T_4 (i.e., XT_{14}) since it is the closest interfering transmitter. Comparing the results for the 3 and 1 dB transmission BWs at the same K, it is clear that the narrower the band of the transmitted signal the smaller the crosstalk. This can be understood from the "notch" shape of the transmission
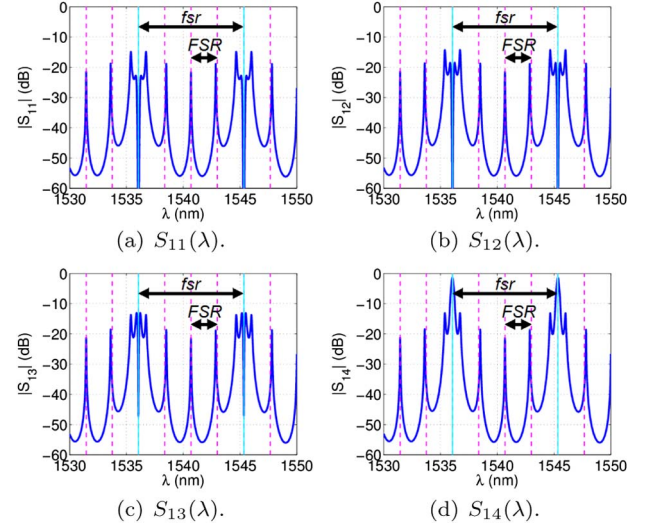
Fig. 3.   Transmission coefficient spectra.

coefficients S_{11}, S_{12}, and S_{13} reported in Fig. 3. Such a crosstalk contribution is approximately −10 dB (−20 dB) when the 3 dB (1 dB) BW is considered for any coupling ratio K larger than 5%.

Figure 5 depicts the behavior of the transmission coefficient S_{14} for increasing values of the radius ρ when the local microring radii are $r = 10$ μm. The figure shows that the resonance of the MMR is determined by the local
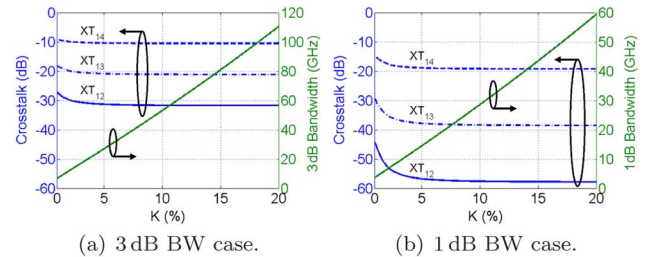
Fig. 4.   BW and corresponding crosstalk with respect to K for $r = 10$ μm and $\rho = 40$ μm.
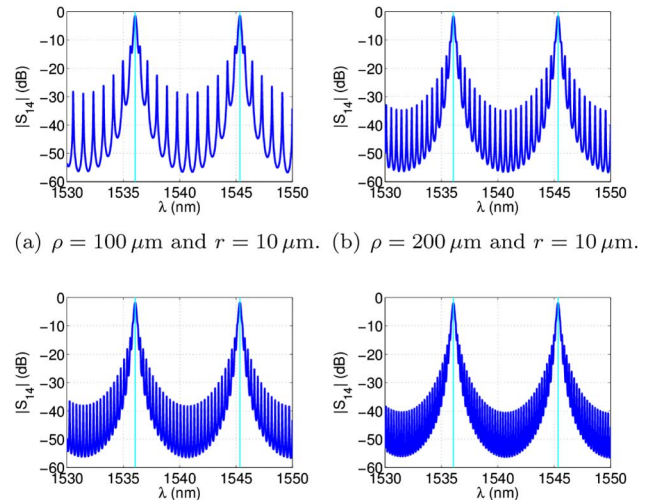
Fig. 5.   Spectra of $S_{14}(\lambda)$ for increasing values of ρ.

(a) Resonant wavelength shift.   (b) SLS vs. K and r.
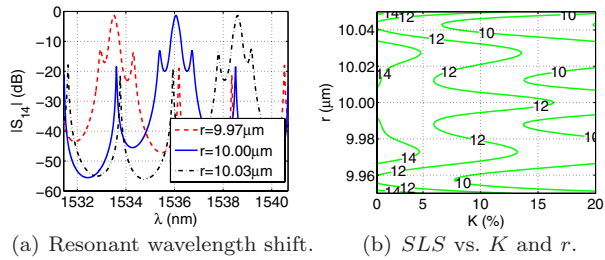
Fig. 6.   Radius inaccuracy analysis. (a) Spectra of $S_{14}(\lambda)$ for different r and $K = 10\%$. (b) Radius inaccuracy and K variation effects on SLS (dB).

(a) 3 dB BW (GHz).   (b) 1 dB BW (GHz).

Fig. 7.   Radius inaccuracy analysis. (a) 3 dB BW and (b) 1 dB BW with respect to K and r.

microring resonance and that the central microring acts basically as a bus connecting the local microrings.

Due to fabrication variability, waveguide cross sections and ring radii may be inaccurate. While variation of the former results in a different effective index, and consequently a change of phase constant β, the latter produces a round-trip distance different from the designed value. As a consequence, the round-trip phases for the local and central microrings ($\phi_r = \beta 2\pi r$ and $\phi_\rho = \beta 2\pi \rho$) are mismatched with respect to the designed specifications, causing a shift of the resonance wavelength. The robustness to fabrication inaccuracies is investigated by changing the radius r of the local microrings. Similar results can be achieved by varying β. This effect is shown in Fig. 6(a) where the spectrum of S_{14} is depicted for different values of r and $K = 10\%$. For radius inaccuracies within ± 30 nm that are within current fabrication tolerance in SOI, the resonance wavelength is shifted up to 3 nm. Such a detuning can be efficiently compensated by thermal trimming [16]. Figure 6(b) shows the variation of sidelobe suppression (SLS) due to the mismatch between the central and local microring radii as a function of K. As can be seen, even for a very large radius inaccuracies (± 30 nm) the SLS is not seriously affected.

The power coupling ratio K is also a critical parameter for microring-based systems. Its value is related to the ring-waveguide distance (gap), which is difficult to precisely control in the fabrication process. The 3 dB and the 1 dB BWs with respect to K are shown in Figs. 7(a) and 7(b), respectively. From the previous results, it is clear that $K = 7.5\%$ guarantees the transmission BW for a 10 Gb/s nonreturn-to-zero on–off keyed signal within the 1 dB BW of S_{14} (i.e., 1 dB BW of 20 GHz) as shown in Fig. 4(a), and it assures a crosstalk of –20 dB. Moreover, for the same value of K, a SLS higher than 11 dB can be achieved regardless of r as shown in Fig. 7(b).

In this work, a multi microring architecture for optical NoC has been presented. Using the transfer matrix method, the input/output transfer matrix has been computed in the case of four transmitters/receivers. The proposed NoC is robust to the inaccuracies that typically occur during the fabrication, leading to a variation of the
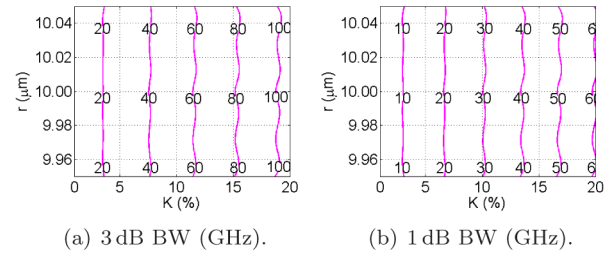
power coupling coefficients and microring radii. Finally, a crosstalk of about –20 dB has been demonstrated when the signal spectrum falls within the 1 dB BW of the transmission coefficient S_{14}.

References

1. J. Kim, K. Choi, and G. Loh, IEEE J. Emerg. Sel. Topics Circuits Syst. **2**, 124 (2012).
2. L. P. Carloni, P. Pande, and Y. Xie, in *Proceedings of the ACM/IEEE Intenational Symposium on Networks-On-Chip* (IEEE, 2009), pp. 93–102.
3. A. Shacham, K. Bergman, and L. P. Carloni, IEEE Trans. Comput. **57**, 1246 (2008).
4. O. Liboiron-Ladouceur, I. Cerutti, P. G. Raponi, N. Andriolli, and P. Castoldi, IEEE J. Sel. Top. Quantum Electron. **17**, 377 (2011).
5. N. Sherwood-Droz, H. Wang, L. Chen, B. G. Lee, A. Biberman, K. Bergman, and M. Lipson, Opt. Express **16**, 15915 (2008).
6. P. Pintus, P. Contu, N. Andriolli, I. Cerutti, and P. G. Raponi, in *Proceedings of the IEEE Optical Interconnects Conference* (IEEE, 2013), pp. 80–81.
7. A. Yariv, Electron. Lett. **36**, 321 (2000).
8. J. Capmany, P. Muñoz, J. D. Domenech, and M. A. Muriel, Opt. Express **15**, 10196 (2007).
9. P. Pintus, P. Contu, N. Andriolli, A. D'Errico, F. Di Pasquale, and F. Testa, J. Lightwave Technol. **31**, 3943 (2013).
10. B. E. Little, J.-P. Laine, and S. T. Chu, Opt. Lett. **22**, 4 (1997).
11. G. C. Ballesteros, J. Matres, J. Martí, and C. J. Oton, Opt. Express **19**, 24980 (2011).
12. I. Davis, *Circulant Matrices* (Wiley 1979).
13. J. Jin, *The Finite Element Method in Electromagnetics*, 2nd ed. (Wiley Interscience, 2002).
14. S. K. Selvaraja, P. Jaenen, W. Bogaerts, D. Van Thourhout, P. Dumon, and R. Baets, J. Lightwave Technol. **27**, 4076 (2009).
15. S. Feng, T. Lei, H. Chen, H. Cai, X. Luo, and A. W. Poon, Laser Photon. Rev. **6**, 145 (2012).
16. M. R. Watts, W. A. Zortman, D. C. Trotter, G. N. Nielson, D. L. Luck, and R. W. Young, *Proceedings of the Conference on Lasers and Electro-Optics/Quantum Electronics and Laser Science Conference* (2009), paper CPDB10.